Journal of
Polymer Materials

Tech Science Press

https://doi.org/10.32604/jpm.2026.077304

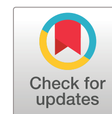

ARTICLE

Research on the Regulation of Polyimide Film Microstructure and Its O_2 Plasma Etching Behavior in the Drying Process

Peishuai Xing[1], Xiaodong Guo[2], Yang Wang[1,*], Sixi Zha[1], Zeting Chen[3], Shicheng Shen[1], Bin He[2], Tianyun Li[2] and Yuning Zhao[2]

[1]School of Mechanical Engineering, XinJiang University, Urumchi, China
[2]Semiconductor Technology Research Department, Ji Hua Laboratory, Foshan, China
[3]South China Academy of Advanced Optoelectronics, South China Normal University, Guangzhou, China

*Corresponding Author: Yang Wang. Email: wy830052@126.com

Received: 06 December 2025; Accepted: 31 January 2026; Published: 30 June 2026

ABSTRACT: In the fabrication of microelectronic devices, polyimide (PI) is often patterned through plasma etching. However, the relationship between its etching behavior and the precursor processing technology has not been systematically revealed. In this paper, PMDA-ODA type PI was selected as the research object. For the first time, the effects of two film-forming processes, freeze drying (FD) and thermal drying (TD), on the microstructure of PI films and their O_2 plasma etching behavior were systematically compared. By means of scanning electron microscopy (SEM), X-ray photoelectron spectroscopy (XPS), Fourier transform infrared spectroscopy (FTIR), and water contact angle testing, the intrinsic differences between the two types of films and the performance evolution rules during the etching process were clarified. The results show that the surface of the FD-PI film exhibits discrete pore structure, while the TD-PI film is characterized by a dense and non-porous structure. This structural difference leads to more significant surface morphology evolution and chemical composition changes in FD-PI during the etching process. After plasma treatment, polar oxygen-containing groups such as O=C-O were successfully introduced onto the surfaces of both types of films. The content of these groups showed regular changes with the etching time, and the wettability of the films processed by the two different technologies was characterized by a dynamic water contact angle measuring instrument. This study reveals the internal mechanism by which the drying process affects the plasma etching behavior of PI films by regulating their initial microstructure, providing important theoretical basis and process guidance for the precision processing of high-performance PI films for advanced electronic devices.

KEYWORDS: Polyimide films; freeze drying; plasma etching

1 Introduction

Polyimide (PI) has emerged as one of the key materials in the fields of microelectronics and flexible electronics, [1,2] owing to its exceptional thermal stability, mechanical properties, chemical inertness, and dielectric characteristics [3]. It is widely employed in passivation layers of integrated circuits, flexible substrates, stress-buffer coatings, and inter-layer dielectrics of multi-layer interconnect structures [4,5]. In these applications, plasma etching technology is typically utilized to perform high-precision patterning on PI films to achieve the functional structures of devices [6,7]. Therefore, a profound understanding and precise control of the plasma etching behavior of PI are crucial for enhancing device performance and yield [8–10].

Copyright © 2026 The Authors. Published by Tech Science Press. This work is licensed under a Creative Commons Attribution 4.0 International License, which permits unrestricted use, distribution, and reproduction in any medium, provided the original work is properly cited.

However, the etching characteristics of PI are not solely determined by its chemical composition [11–13]. Numerous studies have indicated that its final performance is strongly dependent on the synthesis and curing processes of the precursor, polyamic acid (PAA) [14–17]. Among these processes, drying, as a critical step in the transformation from PAA solution to solid PI film, directly influences the final microstructure of the film, such as molecular chain arrangement, free volume, and porosity [18–22]. The thermal drying (TD) process, which is widely adopted in the industry, causes rapid solvent evaporation at high temperatures, easily resulting in a dense and non-porous film structure [23–25]. In contrast, vacuum freeze drying (FD), as an emerging physical film-forming technology, removes the solvent through sublimation, theoretically better preserving the initial network structure of the PAA solution and thus enabling the preparation of PI films with discrete pore characteristics [26–29].

The structural differences caused by different drying processes are bound to affect the diffusion, adsorption, and reaction kinetics of plasma active species (such as radicals and ions) in the film, thereby having a decisive impact on the etching rate, surface morphology evolution, and chemical composition change [30–33]. Wei et al. [34] employed the freeze drying process, dispersing rGO and PAA in DMAc (dimethylacetamide), freezing the mixture at −80°C for 12 h, and then removing DMAc through freeze drying technology to obtain rGO/PAA films. Subsequently, the obtained films were thermally imidized to form the final rGO/PI films. These PI composite films exhibit good flexibility, excellent thermal stability, and high thermal conductivity. Ding et al. [35] investigated the preparation of porous polyimide (PI) aerogel films through partial pre-imidization processes, combined with surface modification and solvent exchange, using atmospheric drying and freeze drying, respectively. The study explored the regulatory effects of the pre-imidization degree (pre-ID) on the pore structure, density, porosity, dielectric properties, and mechanical properties of the films. It was ultimately confirmed that atmospheric drying can produce porous PI aerogel films with both a low dielectric constant and excellent mechanical strength, providing a feasible solution for their large-scale, low-cost applications. Wang et al. [36] studied the behavior of PI films treated with atmospheric-pressure air plasma at different powers. They found that as the power increased, the surface roughness and wettability of the films improved. High-energy particles in the plasma bombarded the PI surface, breaking chemical bonds (such as C–N) and generating dangling bonds and active sites. These sites reacted with oxygen in the air to form polar functional groups. Insufficient power led to a shortage of active particles, while excessive power might cause over-etching and damage the formed functional groups. However, as the etching power increased, the surface roughness increased accordingly, enhancing the hydrophilicity of the PI film. Zhang and Ionov [37] used PAA as the base, dispersed silica particles of different sizes, to form a stable dispersion liquid. Then, during the drying process, with the assistance of capillary force and gravity, a three-layer structure film was formed: the top layer was a single layer of SiO_2 particles, the middle layer was pure PAA, and the bottom layer was a PAA-SiO_2 composite; finally, by gradually heating and imidization, PAA was converted into PI, and then with hydrofluoric acid (HF) etching, the SiO particles were removed. Eventually, a "solid-porous" vertical gradient-distributed PI film was obtained. This PI film formed after etching has reversible self-folding properties and is suitable for flexible actuators. Although previous studies have separately explored the etching performance of PI or its preparation processes, there is still a lack of a systematic and in-depth understanding of how the drying process directly affects the subsequent plasma etching behavior of PI films by regulating their initial microstructures. This lack of research on the correlation limits the ability to precisely control the downstream etching characteristics through upstream process design.

As summarized in the literature review, existing studies have mainly focused on two aspects: (1) exploring the plasma etching performance of PI films independently, without linking it to the upstream precursor drying process; (2) investigating the preparation of porous PI films via freeze drying or thermal

drying, but failing to systematically reveal how the initial microstructure regulated by drying processes affects subsequent plasma etching behavior. In contrast, this study takes the classic PMDA-ODA type PI as a model system and for the first time systematically compares the microstructure differences between FD-PI and TD-PI films and their intrinsic correlation with O_2 plasma etching behavior. Unlike previous fragmented research, this work clarifies the complete structure-property relationship linking the drying process, initial microstructure, plasma etching behavior, and surface performance. This fills the gap in the field regarding the correlation between upstream film-forming processes and downstream precision etching characteristics. This unique perspective not only provides new theoretical insights into the plasma processing of PI films but also offers practical process guidance for customizing PI film performance through upstream process design in advanced electronic device applications.

2 Experiment

2.1 Materials

The PAA solution was prepared using the following industrial-grade raw materials: p-phenylene terephthalic acid dianhydride (PMDA, purity 99.5%) as the di-anhydride monomer, 4,4′-diaminodiphenyl ether (ODA) as the di-amine monomer, and N,N-dimethylacetamide (DMAc, purity > 99%) as the solvent.

2.2 Polyamide Acid Synthesis

ODA and PMDA monomers were first subjected to vacuum drying at 80°C. As shown in Fig. 1, the PAA synthesis was carried out at 0°C: 2.50 g of ODA was dissolved in 44.8 g of DMAc, and after complete dissolution, 2.73 g of PMDA was gradually added and stirred for reaction to obtain the PAA solution.

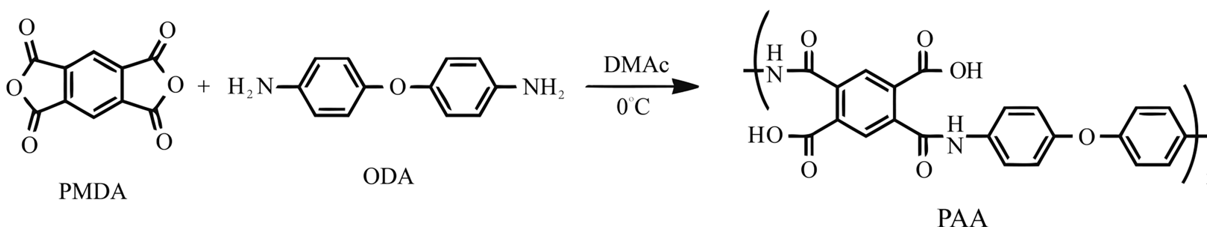

Figure 1: Synthesis process of the polyamide acid (PAA).

2.3 Film Preparation

The PAA solution was coated onto the glass substrate using a vacuum heating knife-line rod integrated coating machine (TBJ-X3-XB), with the wet film thickness controlled at 500 μm. The curing and imidization of the film were carried out using a stepwise heating procedure: heat treatment at 80°C, 120°C, 150°C, and 200°C for 30 min each, followed by treatment at 250°C for 1 h to obtain the thermally dried (TD-PI) film. The vacuum frozen film was prepared by coating the PAA solution onto the glass substrate (wet film thickness 500 μm), and then the sample was pre-frozen at −80°C for 12 h and subsequently transferred to a vacuum freeze drying machine (FTFDS Venus 2.5 L, −55°C) for 36 h. Finally, the imidization of the sample was completed in a vacuum drying box to obtain the vacuum frozen drying (FD-PI) film.

2.4 Plasma Treatment

All PI film samples (FD-PI and TD-PI) were subjected to oxygen plasma treatment using a reactive ion etching machine. The etching parameters were fixed as follows: O_2 flow rate 1000 sccm, Ar flow rate

500 sccm, chamber pressure 180 Pa, and RF power 800 W. To study the effect of time, the etching time was set to 0 (control), 1, 5, and 10 min.

2.5 Characterization Techniques

The surface morphology of the films was characterized using a Thermo Fisher Verios 5 UC type ultra-high resolution field emission scanning electron microscope. To enhance conductivity, all samples were subjected to gold spraying treatment before testing. The surface roughness and topography of the films were analyzed using a Bruker NanoWizard NanoOptics atomic force microscope operated in tapping mode. The scanning area for all measurements was set to 5 μm × 5 μm. The elemental composition and chemical states of the film surfaces were analyzed using a Thermo Scientific Escalab Xi+ XPS equipped with a monochromatic Al Kα X-ray source (hv = 1486.6 eV). Analysis was performed with a spot size of 650 μm, and charge neutralization was achieved using a combination of low-energy electrons and magnetic lens mode to ensure accurate analysis of the insulating PI films. The C1s peak at 284.8 eV was used as the standard for binding energy calibration. The binding energies of relevant functional groups were set as follows: C–N around 285.5 eV, C–O around 286.3 eV, C=O around 288.1 eV, and COO around 289.1 eV. The full width at half maximum (FWHM) of all fitted peaks was constrained within 1.0–1.4 eV,and peaks of the same functional group in different samples maintained consistent FWHM ranges to avoid arbitrary fitting. Similarly, the O1s peak was centered around 532.0 eV, and the N1s peak was centered around 400.0 eV for charge calibration consistency. The spectra were deconvoluted using Avantage analysis software to quantitatively analyze the types and content changes of surface functional groups. The pore size of the freeze-dried microstructure was analyzed using ImageJ software. The chemical structure and imidization degree of the films were confirmed using the attenuated total reflection (ATR) mode of a GD FTIR-850 Fourier transform infrared spectrometer. The wetting properties of the film surfaces were evaluated at room temperature using the sessile drop method with a Dataphysics dynamic contact angle measurement instrument. A deionized water droplet volume of 0.06 mL was used for all measurements. The droplet morphology was captured in real-time by the instrument's built-in image analysis system, and the contact angle value was accurately calculated to quantify differences in surface hydrophobicity and to evaluate the regulation effect of plasma etching on wetting properties. To clarify the regulatory effect of O_2 plasma etching time on the mechanical behavior of PI films prepared by different drying processes, tensile tests were conducted using a 100 kN electronic universal testing machine. Prior to testing, all PI film samples were uniformly cut into dimensions of 100 mm × 20 mm to ensure consistent stress distribution during stretching. The tensile test was performed at a constant speed of 5 mm/min.

3 Result and Discussion

3.1 Testing the Drying Effect of Polyimide Films

Fourier transform infrared spectroscopy (FTIR) was employed to analyze PI films subjected to thermal drying and freeze drying. In Fig. 2, the characteristic absorption peaks at 1776 cm^{-1}, attributed to the asymmetric stretching vibration of C=O, and at 1722 cm^{-1}, corresponding to the symmetric stretching vibration of C=O, were both quite prominent [38]. Meanwhile, the characteristic signals at 1374 cm^{-1}, originating from the vibration of the C–N bond in the imide ring, and at 724 cm^{-1}, belonging to the bending vibration of C=O in the imide ring, were also clearly distinguishable, indicating that the PI samples had been thoroughly dried [39]. Additionally, no obvious and sharp absorption peak corresponding to the C=O stretching vibration in the DMAc solvent was observed around 1664 cm^{-1} in the spectra, suggesting that there was no residual solvent in the dried samples and the drying process had been completely accomplished [40].

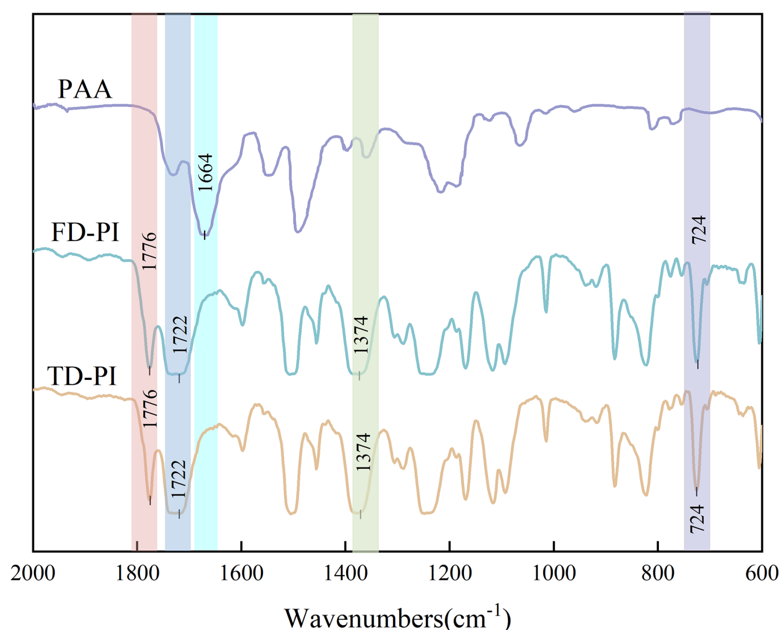

Figure 2: The FTIR spectrum of the PI film after drying (the purple line represents PAA, the blue line represents FD-PI, and the orange line represents TD-PI).

3.2 The Effect of Plasma Treatment Time on the Surface Morphology of Polyimide Films

The initial surface microstructures of PI films prepared by FD-PI and TD-PI were characterized using an ultra-high-resolution field-emission SEM. The morphological changes after O_2 plasma etching of both types of films were compared to reveal the regulatory mechanism of the drying process on the microstructure and etching effect of the films. Figs. 3 and 4 respectively present the SEM images of TD-PI and FD-PI. Before plasma etching, the surface morphologies of the two types of films showed significant differences, with the core difference being the pore characteristics: the surface of TD-PI film was uniform and smooth, with a dense structure, and no obvious pores or protrusions were observed even under a high-magnification microscope (×5000); the morphology was also dense and uniform, and the percentage of cavities was less than 0.5% (calculated by ImageJ software analyzing SEM images), having no significant impact on the overall structural density. This structure originated from the stepwise heating process of thermal drying (80°C–250°C): high temperatures caused the solvent (DMAc) to rapidly vaporize and escape, and the PAA molecular chains rapidly aggregated and closely packed during the solvent evaporation process. The solvent evaporation path was short and there was insufficient space to form stable pores, ultimately solidifying into a dense solid-state PI film. The FD-PI film does not form a continuous porous network, but exhibits 'locally dispersed discrete nanopores'. These non-interconnected nanopores enhance plasma etching effects through two key mechanisms: first, they significantly increase the effective reaction surface area accessible to plasma; second, they provide abundant reaction sites at pore edges and walls. This eliminates the need for interconnected channels to achieve effective etching, as the expanded reaction interface and enriched active sites directly promote the interaction between plasma species and the film. The formed pores were micrometer-sized, with an average pore diameter of 135 nm, and the overall porosity was approximately 8.7%, which was higher than that of TD-PI (0.5%), but far from the characteristic of a porous network structure. This structure is related to the "solvent sublimation" mechanism of freeze drying. During the −80°C pre-freezing process, the solvent in the PAA solution rapidly solidified into ice crystals. However, the growth of ice crystals was affected by inhomogeneous local concentration and temperature distribution, failing to form

a uniform continuous ice crystal template. Subsequent vacuum sublimation of ice crystals only generated discrete pores in the ice crystal distribution area, leading to uneven pore distribution and no interconnection on the film surface.

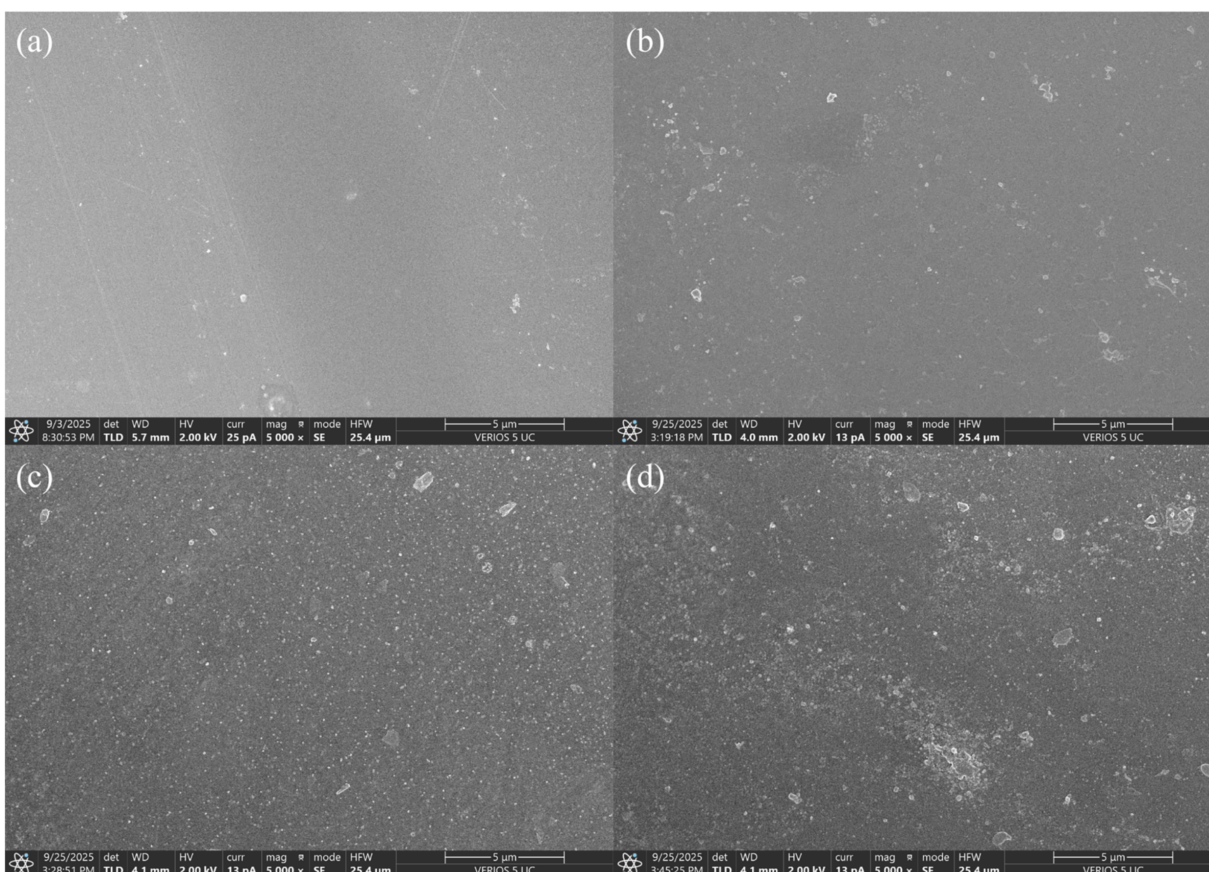

Figure 3: SEM images of TD-PI at different treatment times: (**a**) pristine film (**b**) 1 min (**c**) 5 min (**d**) 10 min.

In terms of structural stability after etching: neither of the two types of films showed significant structural damage. TD-PI maintained its overall dense feature, and the discrete pore structure of FD-PI also did not collapse, still retaining a certain degree of surface structural diversity, which provides a structural basis for subsequent interface functional adaptation.

In conclusion, although the PI films prepared by freeze drying did not form a uniform porous network structure, compared to the completely dense films obtained by thermal drying, the surface-dispersed discrete pores of FD-PI significantly increased the effective reaction surface area accessible to plasma and provided abundant reaction sites. These two effects together enhanced the interaction efficiency between plasma active particles and the film, enabling FD-PI to exhibit higher etching rates and more uniform etching effects. This outcome, from the perspective of microscopic morphology, confirms that the drying process directly affects the interaction efficiency between active particles and the film during plasma etching by regulating the initial pore characteristics of the films, and ultimately determines the etching effect. This provides a key experimental basis for optimizing the PI film coating process for high-precision processing requirements.

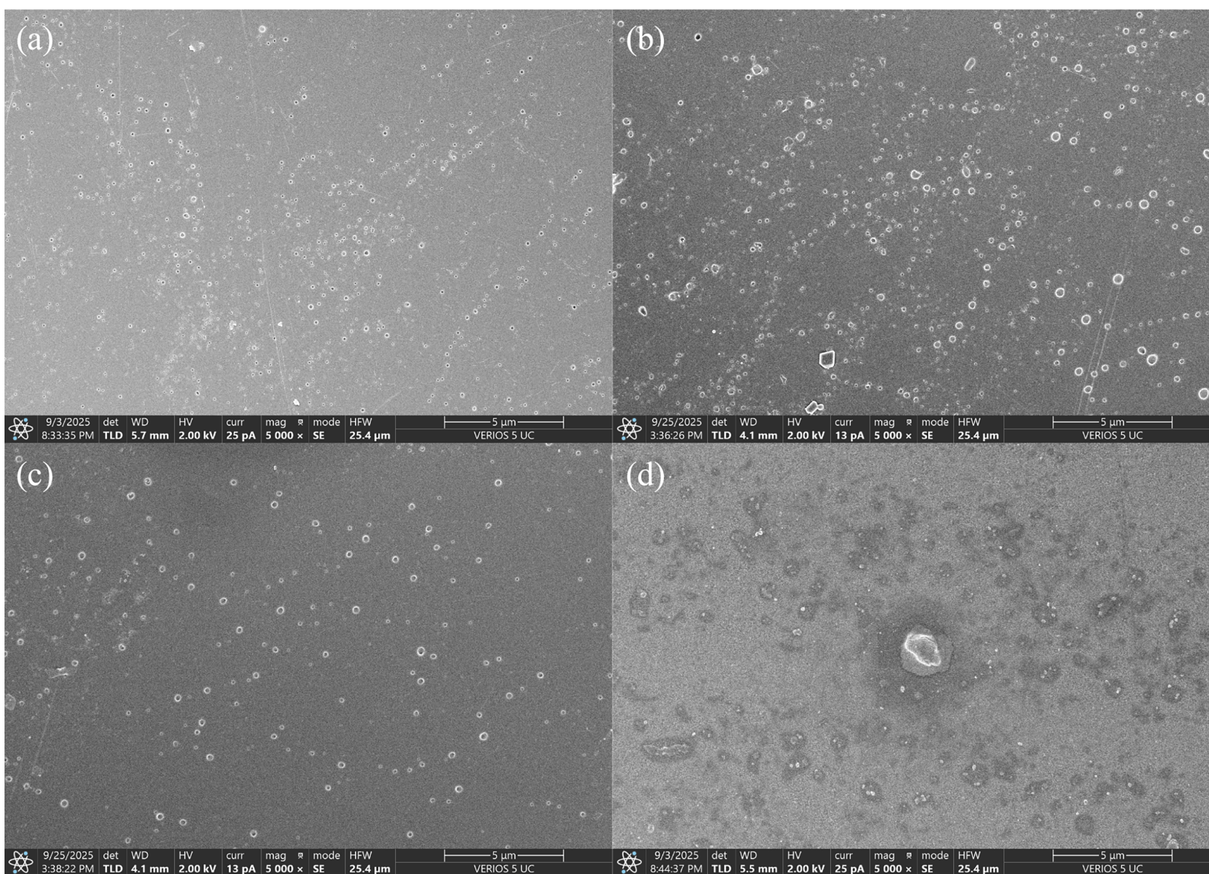

Figure 4: SEM images of FD-PI at different treatment times: (**a**) pristine film (**b**) 1 min (**c**) 5 min (**d**) 10 min.

3.3 The Effect of Plasma Treatment Time on the Surface Roughness of Polyimide Films

To quantitatively evaluate the influence of plasma etching duration on the surface roughness of PI films, AFM was used to test the arithmetic mean roughness (Ra) and root mean square roughness (Rq) of FD-PI and TD-PI films before and after plasma treatment. Figs. 5 and 6 show the AFM images of TD-PI and FD-PI films, respectively, while the AFM 3D images are shown in Figs. S1 and S2 of the supporting documents, respectively.

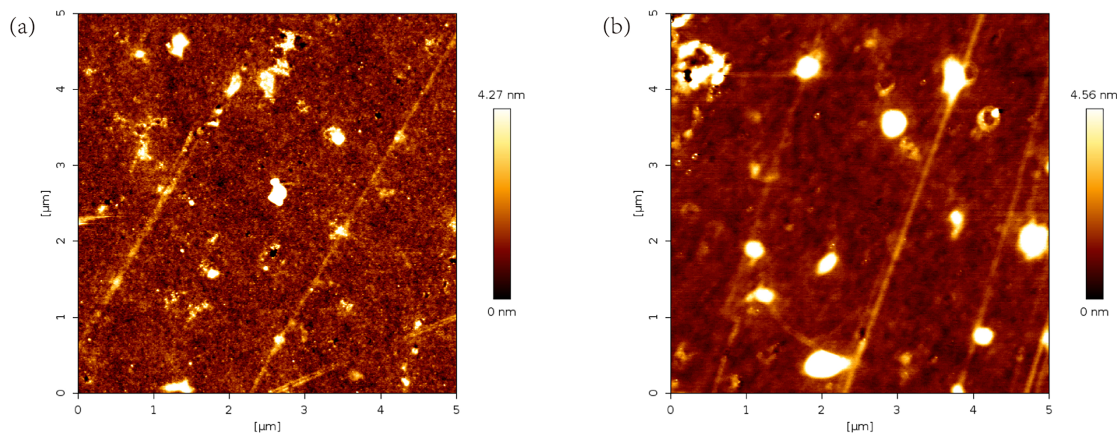

Figure 5: (Continued)

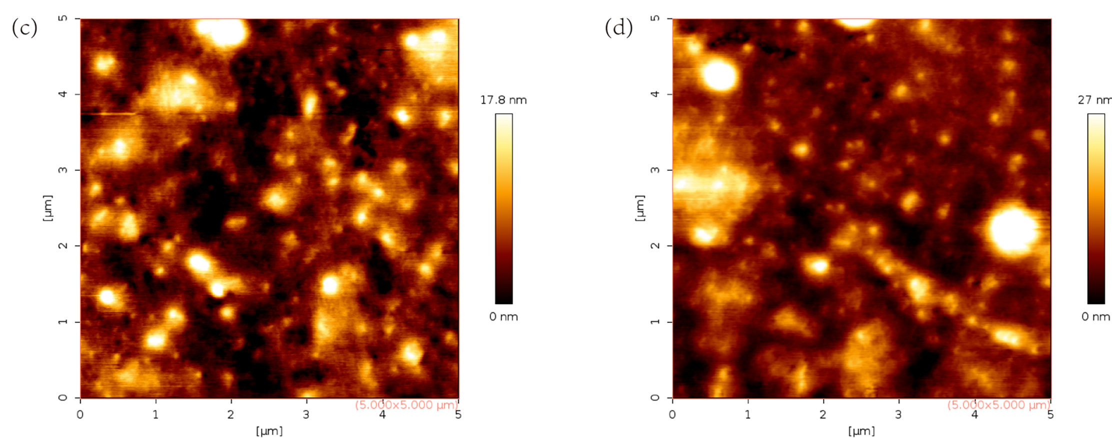

Figure 5: AFM images of TD-PI at different treatment times: (**a**) pristine film (**b**) 1 min (**c**) 5 min (**d**) 10 min.

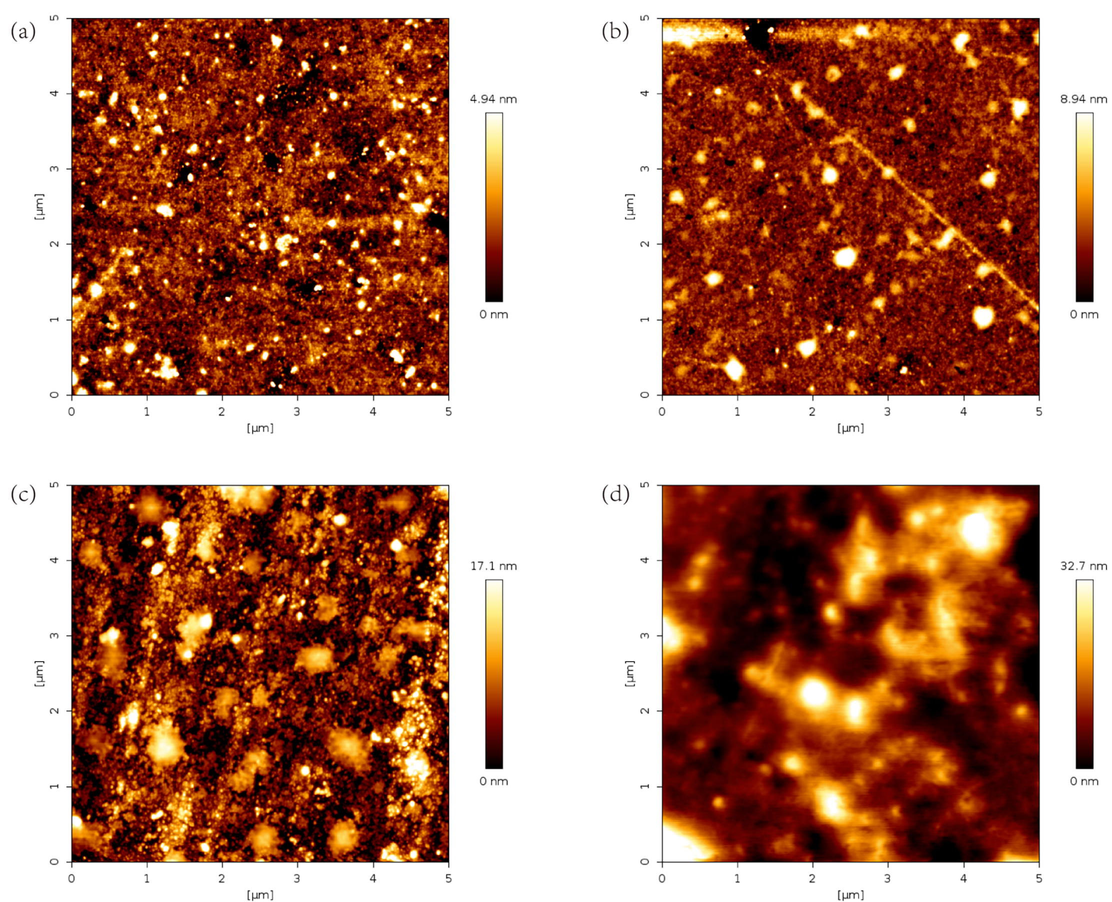

Figure 6: AFM images of FD-PI at different treatment times: (**a**) pristine film (**b**) 1 min (**c**) 5 min (**d**) 10 min.

The surface roughness data of both films under different plasma treatment times are shown in Table 1. Before plasma etching (treatment time = 0 min), the initial surface roughness of the two films already showed obvious differences. The TD-PI film exhibited lower initial roughness: its Ra was 0.407 nm and Rq was 0.969 nm, indicating a smooth and flat surface. In contrast, the FD-PI film, which has a locally dispersed

discrete pore structure, had higher initial roughness (Ra = 0.707 nm, Rq = 1.123 nm). This difference is directly attributed to the discrete pores distributed on the surface of FD-PI, which cause slight undulations in the film surface, consistent with the microstructure characteristics observed by SEM.

Table 1: Effect of plasma treatment times on the surface roughness of different PI films.

	Etching Time (min)	Ra (nm)	Rq (nm)
TD-PI	0	0.407	0.969
TD-PI	1	0.527	1.036
TD-PI	5	2.920	4.038
TD-PI	10	3.98	6.147
FD-PI	0	0.707	1.123
FD-PI	1	1.044	2.034
FD-PI	5	2.975	3.882
FD-PI	10	5.60	7.43

With the extension of plasma treatment time, the surface roughness of both FD-PI and TD-PI films showed a continuous increasing trend, but the growth rate and final roughness value differed significantly. After 1 min of etching, the Ra and Rq of TD-PI increased slightly to 0.527 and 1.036 nm, respectively, while those of FD-PI increased more obviously to 1.044 and 2.034 nm. When the etching time was extended to 5 min, the roughness of both films increased further: TD-PI's Ra and Rq reached 2.920 and 4.038 nm, and FD-PI's Ra and Rq were 2.975 and 3.882 nm. After 10 min of etching, the surface roughness of both films reached the highest level in the test: TD-PI's Rq was 6.147 nm, while FD-PI's Rq reached 7.43 nm, which was 1.21 times that of TD-PI.

The different roughness evolution trends between the two films are closely related to their initial microstructures and etching behaviors. For TD-PI, the dense structure blocks the penetration of plasma active particles, resulting in mild and uneven etching on the surface, so the roughness increases slowly. For FD-PI, the discrete pores significantly increase the effective reaction surface area accessible to plasma and provide additional reaction sites for active particles, enabling more sufficient and uniform etching on the surface.

In summary, plasma treatment time is a key factor regulating the surface roughness of PI films, and the initial microstructure determined by the drying process significantly affects the roughness evolution law. The FD-PI film, with its discrete pore structure, exhibits a more sensitive roughness response to plasma etching, while the TD-PI film with a dense structure shows a relatively gentle roughness change. This quantitative roughness data not only supplements the morphological observation results of SEM but also provides a precise reference for optimizing the surface topography of PI films through plasma treatment for specific application scenarios.

3.4 The Effect of Plasma Treatment Time on the Functional Groups of Polyimide Films

Through XPS analysis, the regulatory effect of plasma treatment on the C1s chemical bond states of the surfaces of two different PI films was systematically investigated. The C1s split peak spectra of the original films prepared by two drying methods and the films after plasma treatment for different durations are presented in the Fig. 7. The results show that plasma treatment significantly altered the composition and relative intensities of the chemical bonds on the surfaces of the two types of films through the interaction between active particles and the film surfaces, successfully introducing new polar oxygen-containing

groups—among which the O=C–O group was mainly attributed to carboxyl groups (–COOH). This is because high-energy active oxygen species in the plasma first break the C–C and C–N bonds on the PI surface to generate dangling bonds, and then these active sites further react with oxygen to form stable –COOH groups. The content of these groups changed regularly with the treatment time, and both the drying method and treatment parameters jointly influenced the reconstruction effect of the surface chemical structure.

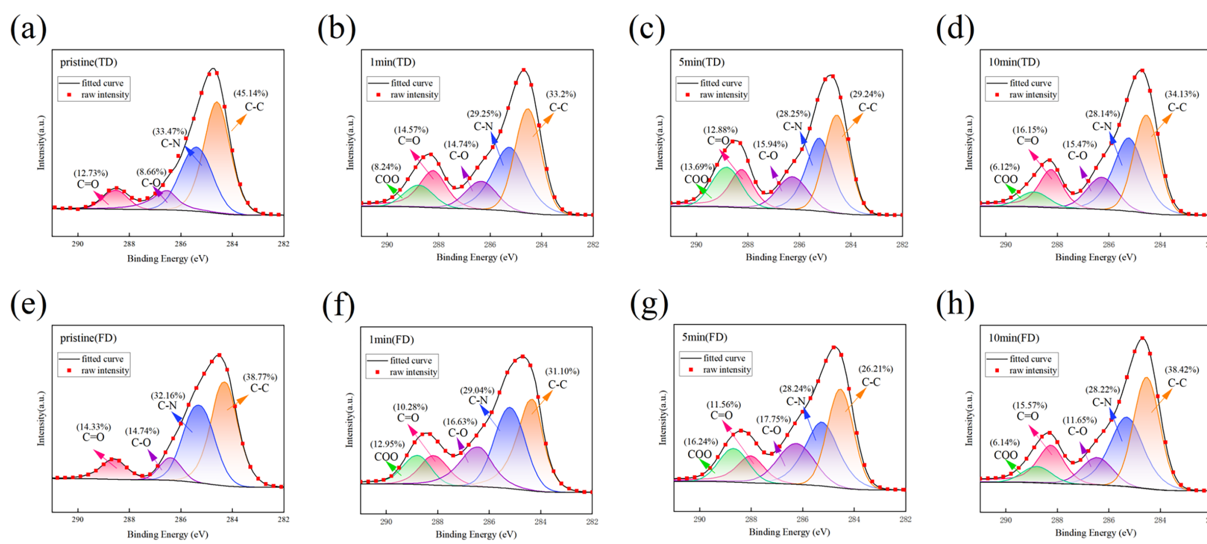

Figure 7: C1s spectra of the PI membrane surface before and after plasma treatment at different times: (**a**) pristine TD-PI (**b**) 1min TD-PI (**c**) 5min TD-PI (**d**) 10min TD-PI (**e**) pristine FD-PI (**f**) 1min FD-PI (**g**) 5min FD-PI (**h**) 10min FD-PI.

The surfaces of the pristine FD-PI film and the pristine TD-PI were mainly composed of four chemical bonds: C–C, C–N, C–O, and C=O. The relative contents of each group in the pristine thermally dried film were 45.14%, 33.47%, 8.66%, and 12.73%, respectively, while those in the pristine freeze-dried film were 38.77%, 32.16%, 14.74%, and 14.33%, respectively. No O=C–O group was detected on the surfaces of both types of pristine films, indicating that without plasma treatment, regardless of the drying process used, the surface chemical composition of the PI films was relatively stable, the overall proportion of oxygen-containing groups was relatively low, and the freeze drying treatment did not cause any fundamental differences in the types of surface chemical bonds, but merely provided a basic chemical matrix for subsequent plasma treatment.

After 1 min of plasma treatment, significant chemical bond reconstruction occurred on the surfaces of both types of films, with the changes in the thermally dried film being particularly obvious: the contents of the C–C and C–N groups decreased significantly. Compared with the original state, the content of the C–C group decreased by 11.94%, and the content of the C–N group decreased by 4.22%. Meanwhile, the contents of the C–O and C=O groups increased by 6.08% and 1.84%, respectively. At the same time, due to the reaction between the active oxygen particles in the plasma and the film surfaces, a new O=C–O group appeared on the surfaces of both types of films for the first time, with a relative content of 8.24% in the thermally dried film, confirming that plasma treatment can effectively break the chemical equilibrium of the original films and introduce oxygen-containing polar groups to the surfaces of the films treated by both drying processes.

When the treatment time was extended to 5 min, the contents of the C–C and C–N groups on the surfaces of both types of films further decreased. Compared with the original state, the C–C group decreased by 15.9% and 12.56% in the thermally dried film and the freeze-dried film, respectively, and the C–N group

decreased by 5.22% and 3.92%, respectively, indicating that the high-energy effect of the plasma continuously broke the surface C–C and C–N bonds, forming surface dangling bonds and providing active sites for subsequent oxidation reactions. At this time, the proportions of the O=C–O group in the films prepared by the two different drying methods reached their peaks, being 13.69% and 16.24%, respectively. The fitting results of the C1s spectrum of the freeze-dried film (5 min (FD)) also showed a similar trend, with the contents of other oxygen-containing groups increasing synchronously, indicating that at this treatment time, the oxidation reaction between the plasma and the surfaces of both types of films was the most sufficient, the generation efficiency of the oxygen-containing functional groups reached the optimum, and the freeze drying pretreatment method did not hinder the generation of oxygen-containing groups.

It is worth noting that when the treatment time was extended to 10 min, the contents of the O=C–O group in both types of films did not increase further, but instead showed an inflection point. The contents of the C–N group in both types of films continued to decrease, confirming that the bond breaking around 285.5 eV was still ongoing. The contents of the C=O group increased by 3.42% and 1.24%, respectively, compared with the original films, while the contents of the newly formed O=C–O group decreased to 6.12% and 6.14%, respectively. This phenomenon was due to the excessive etching of the surfaces of both types of films by the high-energy plasma caused by the prolonged treatment time, which not only destroyed some of the formed oxygen-containing functional groups but also caused the etching and decomposition of the groups, and this excessive etching effect was consistent on the surfaces of the films prepared by both drying methods.

Fig. 8 and Table 2 systematically record the effects of O_2 plasma etching time (0, 1, 5, and 10 min) on the relative contents of C, O, and N elements and the atomic ratios of O/C and N/C on the surfaces of two types of PI films: TD-PI and FD-PI. The regulation of O_2 plasma etching on the surface elements of PI films exhibits a distinct time dependence. Within 5 min, the process is dominated by oxidation reactions, which can effectively increase the surface oxygen content and oxidation degree. Beyond 5 min, the system enters an over-etching stage, leading to the loss of oxygen-containing groups and reverse changes in elemental composition. The initial microstructure of the films is the key factor governing the differences in elemental evolution: the discrete pore structure of FD-PI enhances oxidation efficiency while exacerbating nitrogen loss and the impact of over-etching, whereas the dense structure of TD-PI results in more moderate changes in elemental composition. Furthermore, the O/C atomic ratio reaches its peak at 5 min, which is consistent with the maximum content of O=C-O groups observed in XPS analysis. This finding further confirms that 5 min is the optimal etching time for achieving efficient surface oxidation of both types of PI films.

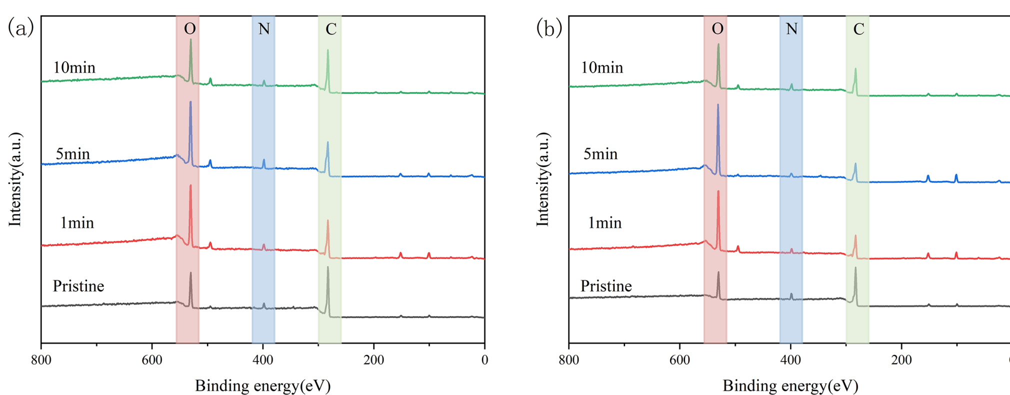

Figure 8: Full spectra of the PI membrane surface before and after plasma treatment at different times: (**a**) TD-PI, (**b**) FD-PI.

Table 2: Effect of plasma treatment times on the relative elemental content of different PI films surface.

	Chemical Composition (%)			Atomic Ratio (%)	
	C	O	N	O/C	N/C
Pristine TD-PI film	76.14	15.63	8.23	20.53	10.81
1 min TD-PI film	68.77	22.02	9.21	32.02	13.39
5 min TD-PI film	62.54	27.31	10.15	43.67	16.23
10 min TD-PI film	68.22	22.98	8.8	33.69	12.9
Pristine FD-PI film	75.58	15.88	8.54	21.01	11.3
1 min FD-PI film	65.53	25.61	8.86	39.08	13.52
5 min FD-PI film	60.92	30.11	8.97	49.42	14.72
10 min FD-PI film	68.18	25.37	6.45	37.21	9.46

3.5 The Effect of Plasma Etching on the Wettability of Polyimide Films

Surface hydrophilicity is a core indicator reflecting the surface energy and chemical state of materials, directly influencing the interfacial bonding performance between PI films and other functional layers in microelectronic devices and the adaptability for subsequent processing. The results are shown in Figs. 9–11. Before etching, both types of original PI films exhibited hydrophobic characteristics, but there were significant differences in their wettability: the initial water contact angle of the TD-PI film prepared by the thermal drying process was 73.8°, which conformed to the typical hydrophobic characteristics of dense PI films with low surface energy; while the initial water contact angle of the FD-PI film prepared by freeze drying was 69.7°, 4.1° lower than that of the TD-PI film.

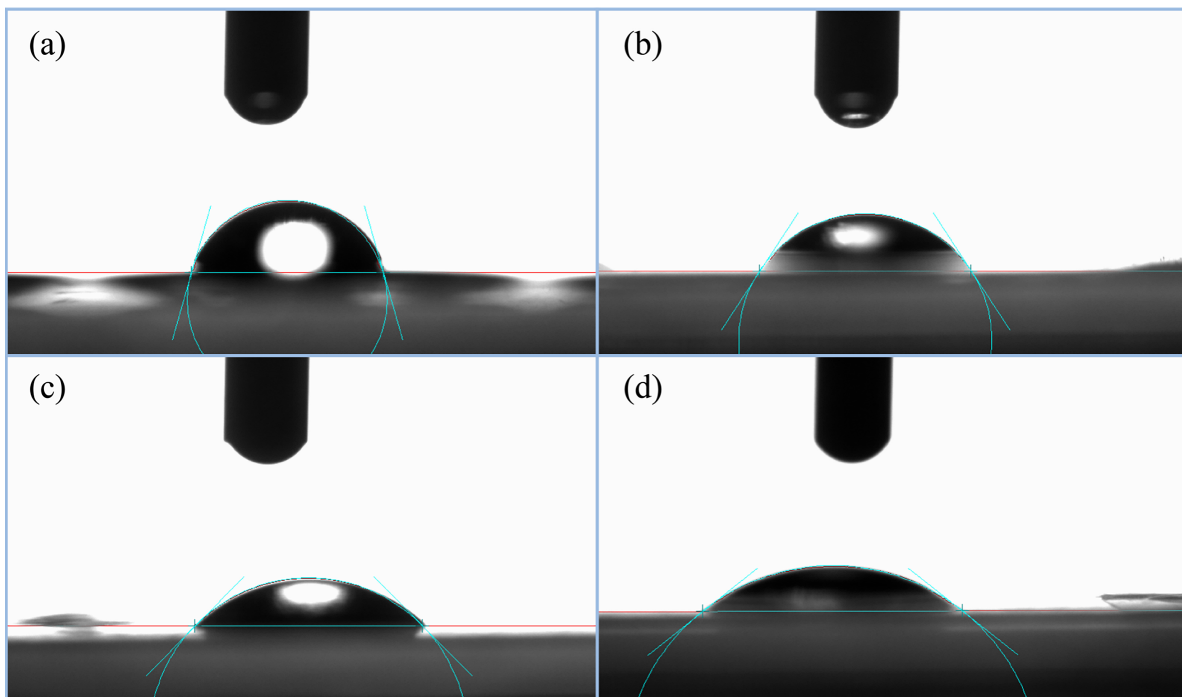

Figure 9: Image of water contact angle of TD-PI film: (**a**) pristine film (**b**) 1 min (**c**) 5 min (**d**) 10 min.

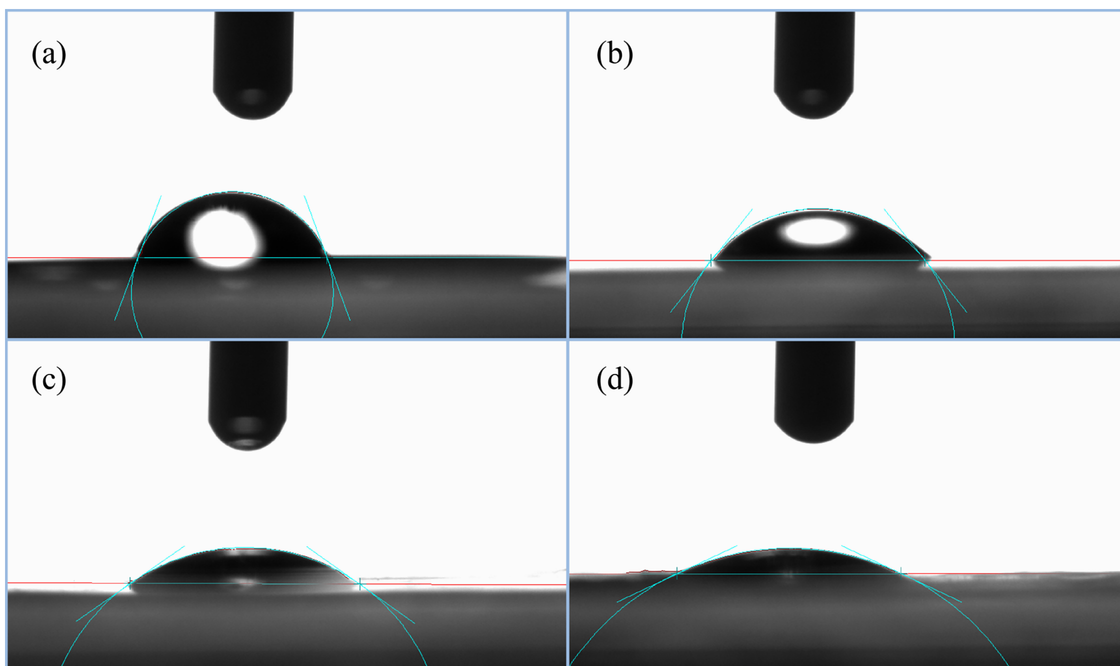

Figure 10: Image of water contact angle of FD-PI film: (**a**) pristine film (**b**) 1 min (**c**) 5 min (**d**) 10 min.

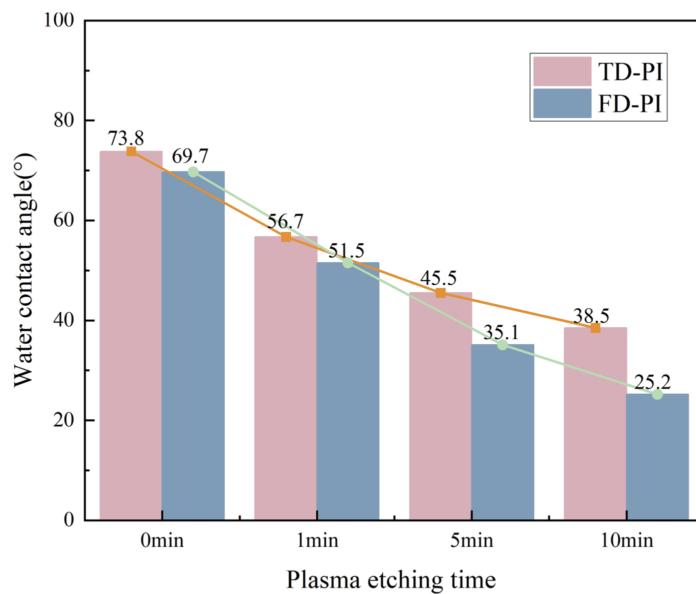

Figure 11: Variation in water contact angle of TD-PI and FD-PI as a function of etching time.

After O_2 plasma etching treatment, the water contact angles of both types of PI films decreased significantly, and with the extension of the etching time, the surface wettability continued to improve: after 1 min of etching, the water contact angles of the TD-PI and FD-PI films decreased to 56.7° and 51.5°, respectively, initially achieving the transformation from hydrophobic to hydrophilic; when the etching time was extended to 5 min, their contact angles further decreased to 45.5° (TD-PI) and 38.1° (FD-PI),

respectively. After the etching time reached 10 min, the water contact angles of the two types of films tended to be stable, being 38.5° (TD-PI) and 25.2° (FD-PI), respectively, both showing excellent hydrophilic performance, and the wettability optimization effect of the FD-PI film was always better than that of the TD-PI film. This fundamental change in wettability can be explained by the "chemical-physical synergistic effect" mechanism: (1) Chemical factors dominate the improvement of hydrophilicity: During the plasma etching process, high-energy active oxygen particles react with the chemical bonds (C–C, C–N) on the PI surface to generate a large number of hydrophilic oxygen-containing polar groups (such as –COOH, –OH). This directly corresponds to the result of "the appearance of the O=C–O group and its content first increases and then stabilizes with the etching time" in the XPS analysis-the introduction of oxygen-containing groups significantly enhances the surface polarity and surface energy, providing a chemical driving force for the spreading of water molecules; (2) Physical factors enhance the wettability effect: Table 1 presents the surface roughness of different PI films measured by atomic force microscopy. As the etching time continues to increase, the surface of the PI film becomes increasingly rough. The surface roughening caused by etching further enhances the hydrophilicity. It is worth noting that the contact angle of the FD-PI film always decreases faster than that of the TD-PI film, and the final contact angle is lower under the same etching time: the contact angle difference was 5.2° after 1 min of etching, and the difference expanded to 7.4° after 5 min of etching, and stabilized at 13.3° after 10 min of etching. The core reason for this phenomenon lies in the discrete pore structure of FD-PI. These discrete pores provide more abundant reaction interfaces for plasma active species, enabling "synchronous modification of the surface and the interior" at the initial etching stage. This avoids the limitation of "preferential surface etching and delayed internal modification" in the dense TD-PI structure, ultimately achieving more efficient and in-depth hydrophilicity regulation. This result further verifies from the perspective of wettability the core conclusion that the drying process determines the plasma treatment effect by regulating the initial microstructure of the PI film, providing an experimental basis for customizing the interface performance of PI films through the film-forming process in the future.

3.6 The Effect of Plasma Treatment Time on the Mechanical Properties of Polyimide Films

The mechanical properties of TD-PI and FD-PI films before and after O_2 plasma etching were evaluated through tensile testing, with the results presented in Figs. 12 and 13, respectively. The tensile strength and strain at break were extracted to assess the impact of etching duration on film integrity and durability.

For TD-PI films, the pristine sample exhibited a tensile strength of approximately 129.96 MPa and a strain at break of about 57%. After 1 min of plasma treatment, the strength decreased slightly to 125.11 MPa, while the strain remained largely unchanged. Prolonged etching to 5 and 10 min led to further reductions in strength, reaching 107.26 and 103.42 MPa, respectively. The strain at break also showed a gradual decline, indicating increased brittleness with extended plasma exposure. The degradation in mechanical performance is attributed to surface and near-surface modification by plasma species, which introduces defects, breaks polymer chains, and reduces structural continuity.

The FD-PI films exhibited a similar trend to TD-PI, with both tensile strength and elongation at break gradually decreased as plasma treatment time increased. However, at the same treatment duration, all mechanical performance metrics of FD-PI were lower than those of TD-PI. This performance discrepancy is primarily attributed to the unique surface-discrete micropore structure of FD-PI films. These discrete micropores inherently act as localized structural defects, which to some extent reduce the intrinsic strength of the material. During plasma treatment, such micropore structures provide additional pathways for active species to penetrate and react, leading to more extensive structural damage on and near the surface of the material, thereby exacerbating the loss of mechanical properties.

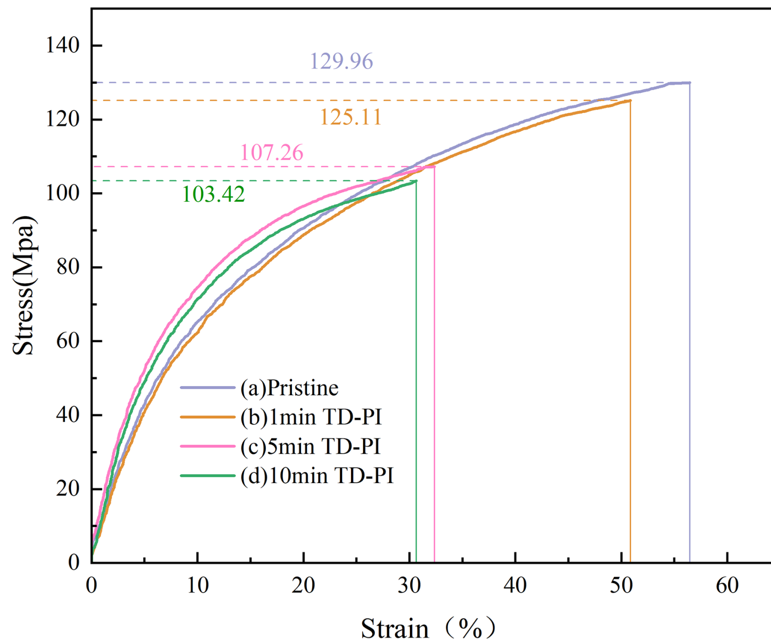

Figure 12: Stress-strain diagram of TD-PI: (**a**) pristine film (**b**) 1 min TD-PI (**c**) 5 min TD-PI (**d**) 10 min TD-PI.

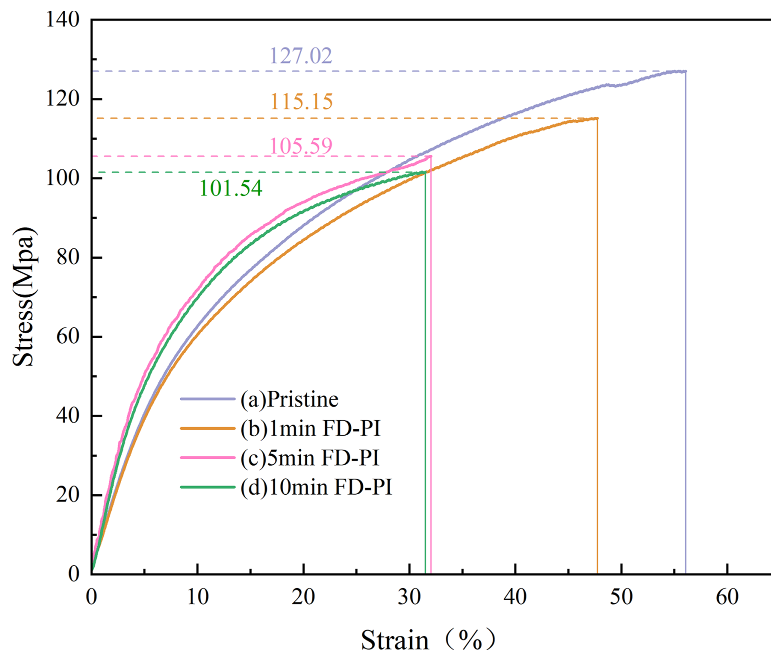

Figure 13: Stress-strain diagram of FD-PI: (**a**) pristine film (**b**) 1 min FD-PI (**c**) 5 min FD-PI (**d**) 10 min FD-PI.

Plasma treatment time significantly regulates the mechanical properties of PI films. The dense TD-PI film exhibits better mechanical stability during etching, while the FD-PI film, despite more significant property degradation, maintains acceptable mechanical performance for practical applications. For advanced

electronic device manufacturing, selecting the appropriate drying process and plasma etching time can achieve a balance between surface functionality and mechanical reliability.

4 Conclusion

This study systematically reveals the intrinsic mechanism by which the drying process of the PAA significantly affects the O_2 plasma etching behavior and final surface properties of PI films through the regulation of their initial microstructures. The research indicates that the FD process successfully introduced a discrete pore structure with uneven distribution, while the TD process forms a dense and non-porous film. This difference in the initial structure is the core reason for the subsequent distinct etching behaviors. During the O_2 plasma etching process, the pores in the FD-PI film provide reaction sites for active species, resulting in a higher etching rate, a more uniform etching morphology, and a more effective bulk modification ability compared to the TD-PI film. Surface chemical analysis confirms that plasma treatment can successfully introduce oxygen-containing polar groups such as O=C-O on the surfaces of both types of films. The content of these groups first increases and then decreased with the treatment time, reaching an optimum at 5 min. However, an excessively long treatment time (10 min) leads to over-etching, causing the decomposition of some oxygen-containing functional groups. The results of the wettability test are highly consistent with the abovementioned structural and chemical evolution patterns: the FD-PI film exhibits a better improvement in hydrophilicity than the TD-PI film during all etching periods. Notably, regulating the plasma etching time enables an optimal balance between the retention of mechanical reliability and the enhancement of surface wettability, catering to the practical application requirements of advanced electronic devices. In summary, this study clarifies the complete structure-property relationship among "drying process-microstructure-etching behavior-surface property". The conclusion clearly points out that the initial microstructure of PI films can be effectively customized through the upstream film-forming process design, providing a new approach and a solid theoretical basis for the on-demand regulation of the downstream plasma precision processing performance. This has important guiding significance for promoting the application of high-performance PI films in advanced electronic devices.

Acknowledgement: The author thanks the Ji Hua Laboratory for providing the experimental equipment for this research.

Funding Statement: This research was funded by National Natural Science Foundation of China (No.: 52202365).

Author Contributions: The authors confirm contribution to the paper as follows: Peishuai Xing: Conceptualization, methodology, software, investigation, formal analysis, writing—original draft; Xiaodong Guo: Data curation, investigation, writing—original draft; Yang Wang: Writing—review and editing, visualization, investigation; Sixi Zha: Supervision; Zeting Chen: Resources, supervision; Shicheng Shen: Software, validation; Bin He: Visualization; Tianyun Li: Supervision; Yuning Zhao: Supervision. All authors reviewed and approved the final version of the manuscript.

Availability of Data and Materials: Not applicable.

Ethics Approval: Not applicable.

Conflicts of Interest: The authors declare no conflicts of interest.

Supplementary Materials: The supplementary material is available online at https://www.techscience.com/doi/10.32604/jpm.2026.077304/s1.

References

1. Wan B, Dong X, Yang X, Wang J, Zheng MS, Dang ZM, et al. Rising of dynamic polyimide materials: a versatile dielectric for electrical and electronic applications. Adv Mater. 2023;35(39):e2301185. doi:10.1002/adma.202301185.
2. Dong Z, He Q, Shen D, Gong Z, Zhang D, Zhang W, et al. Microfabrication of functional polyimide films and microstructures for flexible MEMS applications. Microsyst Nanoeng. 2023;9(1):31. doi:10.1038/s41378-023-00503-5.
3. Liaw DJ, Wang KL, Huang YC, Lee KR, Lai JY, Ha CS. Advanced polyimide materials: syntheses, physical properties and applications. Prog Polym Sci. 2012;37(7):907–74. doi:10.1016/j.progpolymsci.2012.02.005.
4. Li X, Zheng R, Wang C, Chang H, Chen S, Wang L, et al. Preparation and properties of low-dielectric polyimide films containing tert-butyl. Polymers. 2024;16(7):984. doi:10.3390/polym16070984.
5. Sharifi H, Lahiji RR, Lin HC, Ye PD, Katehi LPB, Mohammadi S. Characterization of parylene-N as flexible substrate and passivation layer for microwave and millimeter-wave integrated circuits. IEEE Trans Adv Packag. 2009;32(1):84–92. doi:10.1109/TADVP.2008.2006760.
6. Zawierta M, Martyniuk M, Jeffery RD, Putrino G, Keating A, Silva KKMBD, et al. Control of sidewall profile in dry plasma etching of polyimide. J Microelectromech Syst. 2017;26(3):593–600. doi:10.1109/JMEMS.2017.2681106.
7. Endo A, Takada M, Adachi K, Takasago H, Yada T, Onishi Y. Material and processing technologies of polyimide for advanced electronic devices. J Electrochem Soc. 1987;134(10):2522–7. doi:10.1149/1.2100235.
8. Ji D, Li T, Hu W, Fuchs H. Recent progress in aromatic polyimide dielectrics for organic electronic devices and circuits. Adv Mater. 2019;31(15):1806070. doi:10.1002/adma.201806070.
9. Ni HJ, Liu JG, Wang ZH, Yang SY. A review on colorless and optically transparent polyimide films: chemistry, process and engineering applications. J Ind Eng Chem. 2015;28:16–27. doi:10.1016/j.jiec.2015.03.013.
10. Phan LT, Yoon SM, Moon MW. Plasma-based nanostructuring of polymers: a review. Polymers. 2017;9(9):417. doi:10.3390/polym9090417.
11. del Campo A, Arzt E. Fabrication approaches for generating complex micro- and nanopatterns on polymeric surfaces. Chem Rev. 2008;108(3):911–45. doi:10.1021/cr050018y.
12. Khan AA, Nguyen TK, Trinh QT, Nguyen NT, Dao DV, Zhu Y. Wafer bonding technologies for microelectromechanical systems and 3D ICs: advances, challenges, and trends. Adv Eng Mater. 2025;27(20):2500342. doi:10.1002/adem.202500342.
13. Sezer Hicyilmaz A, Celik Bedeloglu A. Applications of polyimide coatings: a review. SN Appl Sci. 2021;3(3):363. doi:10.1007/s42452-021-04362-5.
14. Jo BW, Ahn KH, Lee SJ. Effect of thermal history during drying and curing process on the chain orientation of rod-shaped polyimide. Polymer. 2014;55(22):5829–36. doi:10.1016/j.polymer.2014.09.016.
15. Rhee S, White JL. Crystal structure, morphology, orientation, and mechanical properties of biaxially oriented polyamide 6 films. Polymer. 2002;43(22):5903–14. doi:10.1016/S0032-3861(02)00489-5.
16. de Ruijter C, Mendes E, Boerstoel H, Picken SJ. Orientational order and mechanical properties of poly(amide-block-aramid) alternating block copolymer films and fibers. Polymer. 2006;47(26):8517–26. doi:10.1016/j.polymer.2006.10.006.
17. Nagella SR, Ha CS. Structural designs of transparent polyimide films with low dielectric properties and low water absorption: a review. Nanomaterials. 2023;13(14):2090. doi:10.3390/nano13142090.
18. Hong D, Lee YJ, Jeon OS, Lee IS, Lee SH, Won JY, et al. Humidity-tolerant porous polymer coating for passive daytime radiative cooling. Nat Commun. 2024;15(1):4457. doi:10.1038/s41467-024-48621-6.
19. Sun X, Di M, Liu J, Gao L, Yan X, He G. Continuous covalent organic frameworks membranes: from preparation strategies to applications. Small. 2023;19(44):e2303757. doi:10.1002/smll.202303757.
20. Chen PJ, Liu TJ, Wu PY, Tseng CF, Leu CM. Drying-induced birefringence of polyimide optical films. AlChE J. 2010;56(3):790–800. doi:10.1002/aic.12022.
21. Unsal E, Cakmak M. Real-time characterization of physical changes in polyimide film formation: from casting to imidization. Macromolecules. 2013;46(21):8616–27. doi:10.1021/ma401361w.
22. Zhang K, Yu Q, Zhu L, Liu S, Chi Z, Chen X, et al. The preparations and water vapor barrier properties of polyimide films containing amide moieties. Polymers. 2017;9(12):677. doi:10.3390/polym9120677.

23. Beck Tan NC, Wu WL, Wallace WE, Davis GT. Interface effects on moisture absorption in ultrathin polyimide films. J Polym Sci Part B Polym Phys. 1998;36(1):155–62. doi:10.1002/(SICI)1099-0488(19980115)36:1155::AID-POLB17>3.0.CO;2-B.
24. Coburn JC, Pottiger MT. Thermal curing in polyimide films and coatings. In: Polyimides. Boca Raton, FL, USA: CRC Press; 2018. p. 207–48.
25. Eguchi Y, Unsal E, Cakmak M. Critical phenomenon during drying of semiaromatic, transparent and soluble polyimide cast films: real-time observation of birefringence and other integrated parameters. Macromolecules. 2013;46(18):7488–501. doi:10.1021/ma401209j.
26. Bai Y, Yan C, Li Z, Qin J, Cheng P. Preparation of high-strength polyimide porous films with thermally closed pore property by *in situ* pore formation method. Acta Phys Chim Sin. 2024;40(9):2306010. doi:10.3866/PKU.WHXB202306010.
27. Wu Z, He J, Yang H, Yang S. Progress in aromatic polyimide films for electronic applications: preparation, structure and properties. Polymers. 2022;14(6):1269. doi:10.3390/polym14061269.
28. Xu K. Design of aromatic thermosetting copolyester compositions and blends for thin film applications. Champaign, IL, USA: University of Illinois at Urbana-Champaign; 2002.
29. Wang J, Zhang K, Bogaerts A, Meynen V. 3D porous catalysts for Plasma-Catalytic dry reforming of Methane: how does the pore size affect the Plasma-Catalytic Performance? Chem Eng J. 2023;464:142574. doi:10.1016/j.cej.2023.142574.
30. Huang Y, Yu Q, Li M, Jin S, Fan J, Zhao L, et al. Surface modification of activated carbon fiber by low-temperature oxygen plasma: textural property, surface chemistry, and the effect of water vapor adsorption. Chem Eng J. 2021;418:129474. doi:10.1016/j.cej.2021.129474.
31. Neyts EC. Plasma-surface interactions in plasma catalysis. Plasma Chem Plasma Process. 2016;36(1):185–212. doi:10.1007/s11090-015-9662-5.
32. Attri P, Kumar N, Park JH, Yadav DK, Choi S, Uhm HS, et al. Influence of reactive species on the modification of biomolecules generated from the soft plasma. Sci Rep. 2015;5(1):8221. doi:10.1038/srep08221.
33. Sun J, Chen Q, Qin W, Wu H, Liu B, Li S, et al. Plasma-catalytic dry reforming of CH_4: effects of plasma-generated species on the surface chemistry. Chem Eng J. 2024;498(7):155847. doi:10.1016/j.cej.2024.155847.
34. Wei S, Yu Q, Fan Z, Liu S, Chi Z, Chen X, et al. Fabricating high thermal conductivity rGO/polyimide nanocomposite films via a freeze-drying approach. RSC Adv. 2018;8(39):22169–76. doi:10.1039/c8ra00827b.
35. Ding C, Li R, Yu J, Wang X, Huang P. Synthesis of porous polyimide films with low dielectric constant and excellent mechanical properties by ambient pressure drying. J Mater Sci. 2022;57(20):9480–92. doi:10.1007/s10853-021-06792-3.
36. Wang J, Yang S, Xiao C, Yu Z, Ren R, Xiong X. Effects of atmospheric pressure plasma treatment and its aging behaviors on interfacial strength of PI/PEEK composite film. J Appl Polym Sci. 2025;142(3):e56369. doi:10.1002/app.56369.
37. Zhang Y, Ionov L. Actuating porous polyimide films. ACS Appl Mater Interfaces. 2014;6(13):10072–7. doi:10.1021/am502492u.
38. Lee SC, Tai FC, Wei CH, Yu JI. ATR-FTIR and nanoindentation measurements of PMDA-ODA polyimide film under different curing temperature. Mater Trans. 2007;48(6):1554–7. doi:10.2320/matertrans.mer2007045.
39. Dong H, Dong J, Li X, Zhao X, Xu Q, Zhang J, et al. Preparation of high-temperature resistant polyimide fibers by introducing the p-phenylenediamine into kapton-type polyimide. ACS Appl Polym Mater. 2024;6(4):2371–80. doi:10.1021/acsapm.3c03051.
40. Kotov N, Raus V, Dybal J. Intermolecular interactions in N,N-dimethylacetamide without and with LiCl studied by infrared spectroscopy and quantum chemical model calculations. J Phys Chem B. 2018;122(38):8921–30. doi:10.1021/acs.jpcb.8b05569.